VFCAL Task Status Report

S. Schuwalow* for FCAL Collaboration†

December 5, 2009

Abstract

The effort within VFCAL was focused on the infrastructure necessary for the design and construction of a laser position alignment system with μm accuracy, for sensor tests in the laboratory and in a beam, and the design and test of FE electronics components. In 2009 needed infrastructure was completed and has been extensively used by collaboration, LumiCal sensor prototypes delivered and tested in Cracow, DESY and Tel Aviv laboratories, 2-nd submission 10-bit ADC converter ASIC delivered and successfully tested. Investigation of radiation hard sensors has been continued. For deliverables separate memos has been written. In this paper we summarize the results.

*DESY, Zeuthen, Germany
†http://www-zeuthen.desy.de/ILC/fcal/

1 Introduction

Very forward calorimeters [1] are planned for the future Linear Collider [2] detectors to extend the coverage to small polar angle, to measure precisely the luminosity and to assist beam tuning to optimize the luminosity. The calorimeters must be fine-grained and compact. The innermost BeamCal calorimeter has to withstand harsh radiation conditions and must be readout bunch-by-bunch. To fulfill necessary precision requirements the LumiCal must be positioned extremely precise and the inner acceptance radius must be controlled on μm level. Fig. 1 shows the design of forward region for the ILD [3] detector concept.

The goal of the VFCAL project [4] is to design these special forward calorimeters. Within JRA3 EUDET activity necessary infrastructure for tests of all subcomponents has to be developed. It includes the development of position monitoring on μm level, the design and test of thin sensor planes and fast FE electronics and investigation of radiation hard sensors.
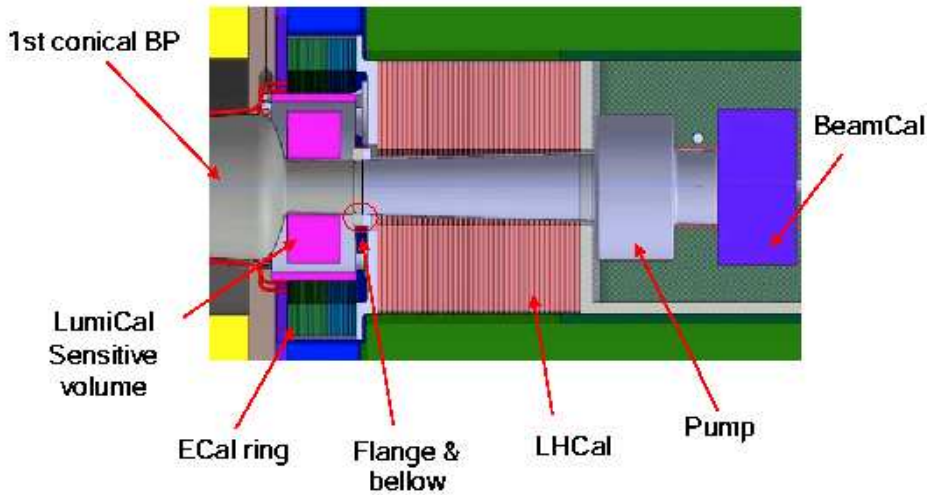

Figure 1: The YZ cross section of the forward region in the ILD detector. LumiCal and BeamCal are centered around the outgoing beam. The detector central region (interaction point) is to the left from the figure.

2 LumiCal Alignment System

To achieve the required precision in luminosity measurement by the LumiCal detector (better than 10^{-3} for $\Delta L/L$ measurements), the following conditions must be met:

- The detector (mechanical frame and internal structure) must be built with micrometer precision.

- The position of each LumiCal with respect to the beam pipe and the distance between the two calorimeters must be controlled with an accuracy of 100 μm.

- Any displacement of its internal layers must be monitored with an accuracy of a few micrometers.

In the following these aspects of R&D LumiCal studies will be presented in more detail.

LumiCal Alignment Studies As the complete LumiCal detector will consist of two Si/W calorimeters placed symmetrically relative to the IP, the alignment procedure will be based on several precise measurements of the calorimeters' positions relative to reference frames, whose positions must be very well known. The measurements will also include the distance between both calorimeters. For the reference frames, the focusing magnet QD0 (which is the last magnet before the IP) or beam line monitors (Beam Position Monitors) can be used. The displacement relative to these reference frames for each of the LumiCal calorimeters should be known within 100 μm for GigaZ and within 700 μm for the luminosity measurement, and the distance between them within 60 - 100 μm. In addition, the inner radius of the sensor layers must be known with an accuracy better than 4 μm. A possible solution for alignment, where one can reach the required high precision in position measurements, is an optical system with laser beams or a method where changes in distance measurements can be observed by measurements of the changes in capacitance at a sensor probe plane. The first tests of the prototypes for both of those methods were successful. This confirms that they can be useful in further development of the alignment system, where a Frequency Scanning Interferometry method will be applied.

The Laser Positioning System based system was built and tested in the laboratory [5, 6]. The main elements were a CCD camera, the laser beams, collimators and filters. Two narrow, collimated laser beams were directed at the sensor of the CCD camera. One is perpendicular to the face of a CCD camera, while the other impinges on it at a 45° angle. As a result, two laser spots appear on the CCD camera and are used in displacement monitoring, where the spot position of the perpendicular beam monitors movements in the (X,Y) plane. The measurements of displacement in the Z direction were obtained from distance measurements between the two spots. The position of the CCD sensor has been controlled by using an optical linear encoder with a resolution of 0.1 μm. Figure 2 shows the system, which was placed within a temperature stabilized box.

After the laser spots are read out, the spot centers are calculated on a computer using an algorithm which takes into account signals in CCD sensor pixels above the background of the electronics noise. The accuracy obtained from measurements was 0.5 μm in the X-Y plane and 1.5 μm in Z direction. This is an order of magnitude better than required. The sensitivity of the system to temperature changes was found to be at the level of 0.5 μm/K over several months of measurements, during which the system worked in a temperature stabilized box. Recent work concentrates on the test of optical CMOS sensor. This smaller system will be applied to automatic readout and position calculations. It will be less sensitive to destruction from the radiation expected in the LumiCal environment, the forward region of ILD.
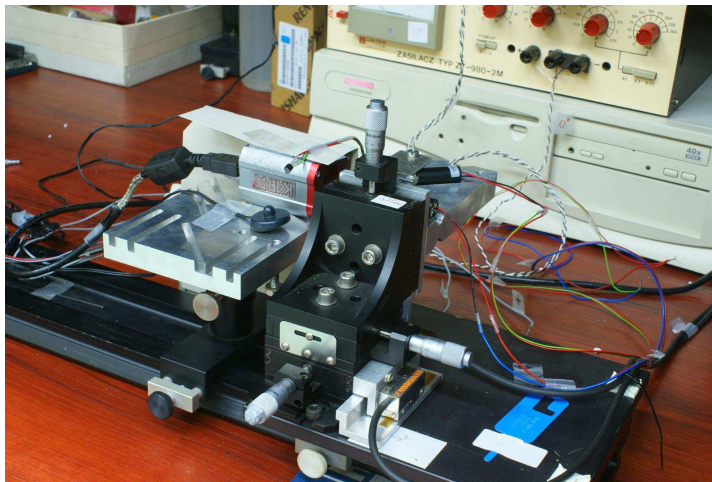
Figure 2: Prototype of the laser position displacement measurement system. Two laser beams from diodes in the rear part of the picture are recorded by a CCD sensor mounted on the movable table in the foreground. For the CCD readout sensor, a specialised FE electronics and DAQ system has been developed.

In the future a more realistic prototype of the laser alignment system (LAS) for LumiCal will be built with lasers using Frequency Scanning Interferometry (FSI) [7, 8, 9, 10] and elements like optical fibers, retro-reflectors, filters and vacuum pipes. The first step in the design of such a system was the estimation of the expected resolution in distance measurements, taking into account the properties of the elements in the system (resolution, stiffness, changes with temperature). This was done using the SIMULGEO program. For measurements of the relative distances to the beam pipe, the precision obtained for X, Y and Z measurements was below 100 μm and below 600 μrad for the modules' rotation angles. The situation becomes more complicated in the case of absolute distance measurements. The precision obtained in reconstruction in that case is on the level of 300 - 600 microns for X, Y and Z measurements. For rotation angles it rises above 800 μrad.

Up to now the laser positioning system used for displacement monitoring considered the LumiCal detector as a whole object. The previously mentioned accuracy requirement for the inner radius of the sensors layers, on the level of 4 μm, emphasizes the problem of finding a method for measuring the displacement of individual sensor layers inside LumiCal with micrometer accuracy. One possible solution is to use a special transparent CMOS sensor placed on each silicon detector layer and an infrared (IR) laser beam traversing all sensor layers. This kind of alignment method (considered for some ILD tracker detectors to monitor detector distortion on the time scale of seconds), using special micro-strip sensors, has been studied before. It was found that resolution on the order of 2 microns can be obtained with this method.

The Capacitance Method In other R&D studies, a capacitive probe system, which can be used for non-contact LumiCal internal sensor layer displacement measurements,

was investigated. The setup consists of a small 5-8 mm^2 flat plane probe, which forms a capacitor to the ground plane that varies with distance. A balanced C-bridge with synchrodetection allows for measurement of the distance in the range 0.5 to 1 mm with an accuracy of 0.5 μm. The electronics are integrated with the capacitive probe to avoid uncertainty due to the probe-electronics cable connection. This method looks very promising and will be used after some improvement to measure the distance of each sensor plane to the beam pipe.

LumiCal and ILD Detector As the LumiCal is part of the ILD detector (Figure 3), several modifications and extensions of the LAS are under study. The system should
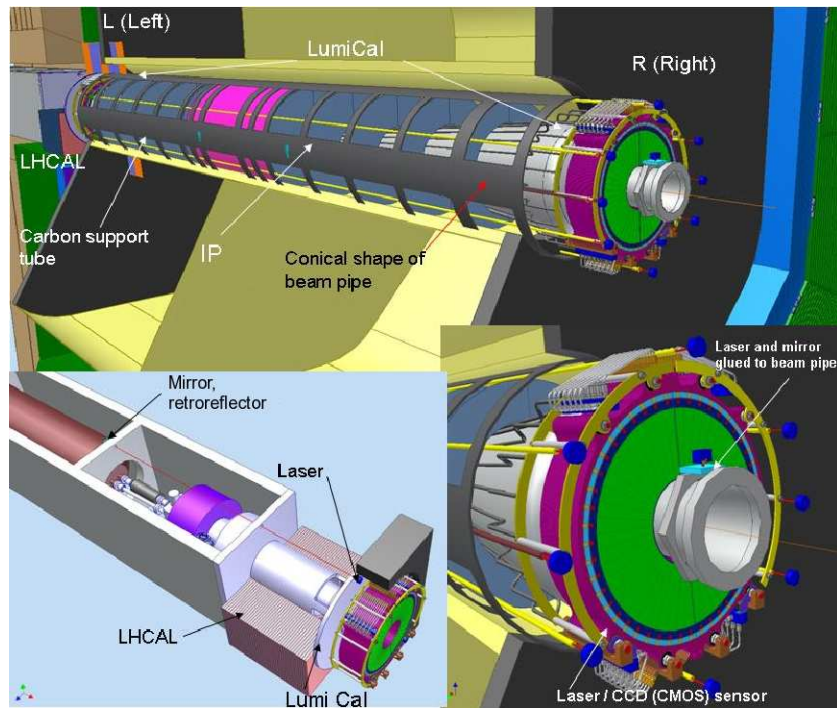

Figure 3: The LumiCal detector inside the ILD detector geometry. The laser beam lines can be used for the distance measurement, both of the calorimeter displacement in respect to the QD0 magnet (or the beam pipe) and the distance measurement between the calorimeters.

allow for the precise displacement measurements of both LumiCal calorimeters with respect to the QD0 magnet or the beam pipe, as well as of the distance between them. To fulfill such requirements additional infrastructure around the beam pipe will be necessary. In a simplified case at least six parallel laser beams (inside additional vacuum pipes) together with CCD (CMOS) sensors and retro-reflectors should be installed on a carbon support tube. In the other version special windows in the beam pipe are considered, where laser beams will cross the support carbon tube. In a more advanced approach the laser positioning system will be based on the frequency scanned interfer-

ometry (FSI) solution which should be part of the global alignment system considered for ILD, including the Vertex detector.

3 Sensor Prototypes

The LumiCal sensitive region extends radially from 80 mm to 195.2 mm. Each sensor layer includes 48 azimuthal sectors. The sectors are placed four to a tile, with 2.5 mm of noninstrumented space between tiles. Each sector is divided radially into 64 cells. The radial cell dimension is $\Delta R = 1.8$ mm, and the azimuthal cell dimension is $\Delta\phi = 7.5°$ (Figure 4). To avoid overlaps of tile gaps every second sensor plane is rotated azimuthally by $\Delta\phi/2$. The silicon sensors will be glued onto a thin Kapton foil (as insulator for
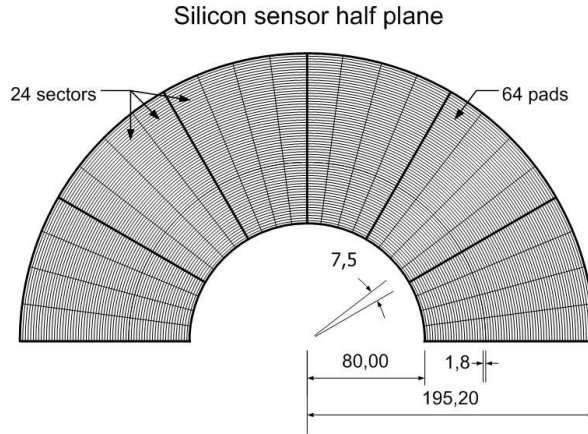

Figure 4: The silicon sensor half plane as planned for the LumiCal calorimeters.

the bias voltage) mounted directly on the tungsten surface of the following absorber. Reference marks are foreseen on the detector surface to allow for precise positioning. The layout of the sensors and the mechanical design of the calorimeter does not allow sensors to overlap. To reduce the impact of the gaps, odd and even planes are rotated by 3.75°. Figure 5 shows the photo of silicon sensor prototype with the structure of 4 sectors and 64 radial pads. Including the 0.6 mm wide guard rings and roughly 0.6 mm clearance for wafer cutting, the inactive gap between the tiles has a width of ≈ 2.5 mm. Monte Carlo simulations show that a gap width up to 2.5 mm does not degrade the precision of the luminosity measurement. 40 such sensors produced by Hamamatsu Photonics have been distributed among three institutes participating in the FCAL Collaboration: Institute of Nuclear Physics PAN (Cracow), DESY (Zeuthen) and Tel Aviv University (Tel Aviv). This insures independent measurements and quality checks of the sensors in each of these institutes. Details of the measurements could be found in [11]. Probe stations developed as a part of EUDET infrastructure project [12] at DESY and Tel Aviv University were used.

As an example of measurements the influence of grounded neighbor pads can be seen in Figure 6. A decrease of the leakage current is measured and the current stays constant
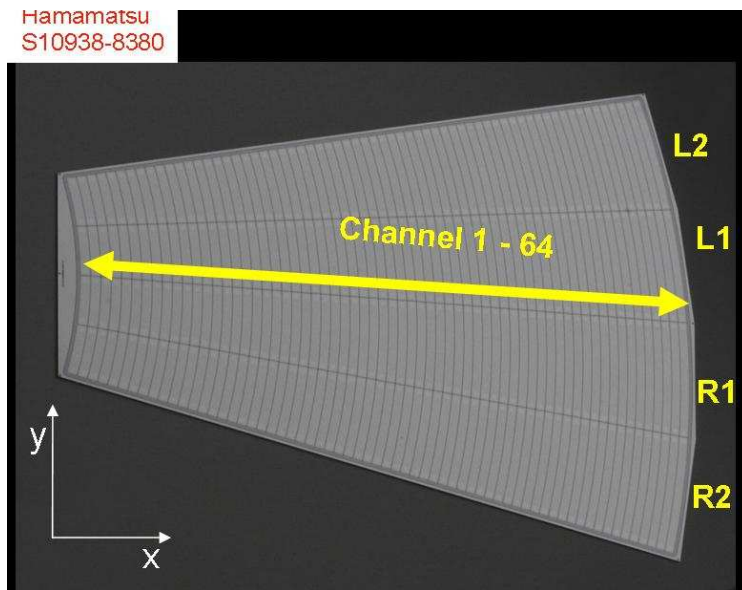
Figure 5: Photo of the silicon sensor prototype for the LumiCal calorimeter.

for a wide voltage range as soon as an electric field below the neighbor pads is applied. The measured leakage current values between 1 and 2 nA in this (regular) case.
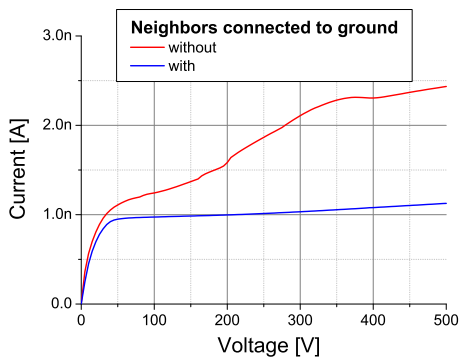

Figure 6: I/V curve for a single pad with and without connected neighbors.
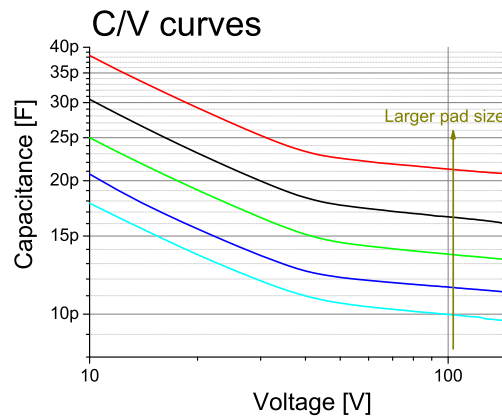

Figure 7: Measured C/V curves.

The C/V curves for several sensor pads are shown in Figure 7. The typical dependence (1/V) of the capacitance (C) on the depletion voltage (V) was found. The capacitances are proportional to the pad size. At a voltage of 150 V the pad capacitance values are 25 pF (largest pad) and 10 pF (smallest pad), respectively. Using these dependencies one can determine the depletion voltage. Values from 39 V to 43 V were found. All the measured values were within the given specifications.

4 Development of the LumiCal Readout Electronics

The design of the LumiCal front end electronics depends on several assumptions and requirements concerning detector architecture. It should work in two modes: physics mode and calibration mode. In physics mode, the detector should be sensitive to high energy deposition from electromagnetic showers, and the front end electronics should process signals up to 10 pC or more per channel. In calibration mode, it should detect signals from relativistic muons – it should be able to register minimum ionizing particles (MIPs). This implies that signals as small as 2 fC (corresponding to the low end of the Landau distribution for MIPs in 300 μm thick silicon) should be detected.

The proposed sensor geometry results in a very wide range of strip capacitances (10 to 100 pF) connected to a single front end channel. Because of the very high expected strip occupancy, the front end should be fast enough to resolve signals from subsequent beam bunches which are separated in time by about 350 ns. Simulations of LumiCal indicate that the reconstruction procedure needs about 10 bit precision on the measurement of the deposited energy. Lastly, power cycling between bunch trains can significantly relax the severe requirements for power dissipation. It is feasible since in the ILC experiment there will be about 200 ms in between each 1 ms long bunch train.

To fulfill the above specifications, the general concept of the full readout chain will comprise front end electronics, a digitizer (ADC) plus zero suppression, and a data concentrator with an optical driver. It has not yet been decided whether a single ADC will serve for one or for several channels.

In the following section the design and measurements of prototype front end electronics and ADC ASICs are presented (a more detailed discussion of the front end and ADC may be found in [13]). The ASIC prototypes have been fabricated in 0.35 μm CMOS technology. The data concentrator has not been designed yet, but since its first prototype is expected to be developed using the FPGA circuits, the development time is expected to be significantly shorter than that of the rest of the readout chain.

Front End Electronics Design The chosen front end architecture includes a charge sensitive amplifier, a pole–zero cancellation circuit (PZC), and a shaper, as shown in Figure 8. In order to cope with large amounts of charge in physics mode and small amounts in calibration mode, variable gain in both the charge amplifier and the shaper is applied. The "mode" switch in Figure 8 changes the effective values of the feedback circuit components (R_f, C_f, R_i, C_i), and therefore changes the transimpedance gain of the front end. Low gain (large C_f) is used for physics mode when the front end processes signals from large charge depositions in the sensor, while high gain (small C_f) is used in the calibration mode when MIP sensitivity is needed.

By setting the PZC parameters properly ($C_\mathrm{f}R_\mathrm{f} = C_\mathrm{p}R_\mathrm{p}$) and equalizing shaping time constants ($C_\mathrm{i}R_\mathrm{i} = C_\mathrm{p}(R_\mathrm{p}||R_\mathrm{s})$), one obtains the first order shaping, equivalent to a CR–RC filter, with a peaking time $T_\mathrm{peak} = C_\mathrm{i}R_\mathrm{i}$. Simple first-order shaping is chosen as a tradeoff between the noise and the power dissipation. Regarding noise, a main requirement is to achieve a signal to noise ratio (S/N) in calibration mode of about 10 for the largest sensor capacitances. Both of the amplifying stages (A_pre, A_sh) are designed
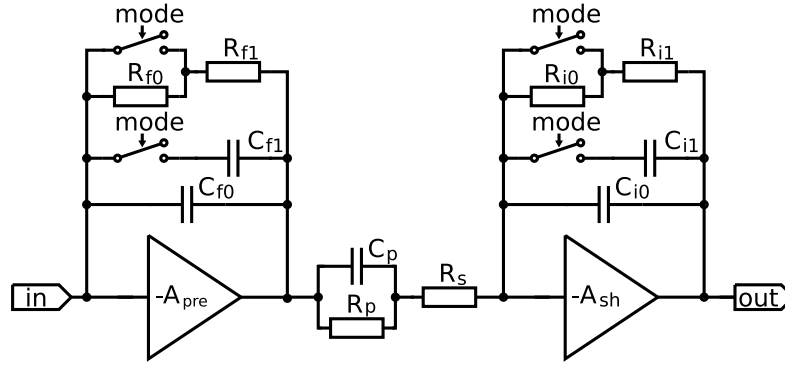
8

Figure 8: Block diagram of a front end channel

as folded cascodes with active loads, followed by the source followers. In the prototype ASIC 8 front end channels are implemented. Four channels are designed with passive feedback and PZC resistances R_f, R_p while the other four channels use MOS transistors in a triode region instead. This allows us to compare the overall performance of the two feedback schemes.

Front-end electronics measurements A photograph of the prototype ASIC, glued and bonded on to the PCB, is shown in Figure 9.
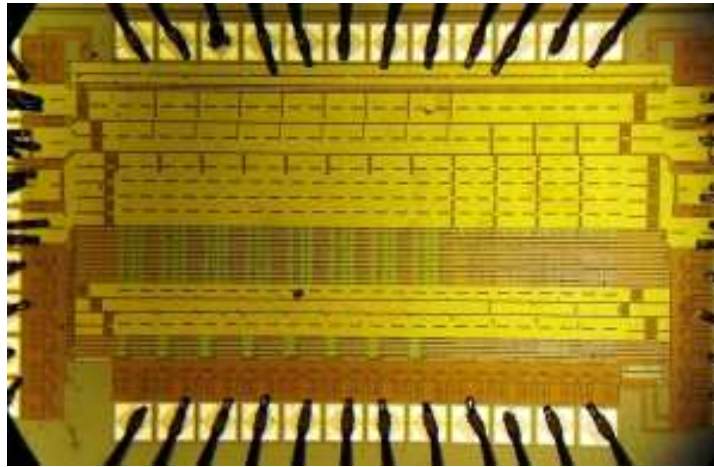
Figure 9: Photograph of glued and bonded FE prototype.

The measured power consumption of about 8.9 mW/channel agrees with simulations. Figure 10 shows the response of the front end channel to charge injected through the input test capacitance for different values of input capacitance (C_{det}) within the range of interest. The sensor capacitance is simulated with an external capacitor. For physics mode the results obtained for active (MOS) and passive (R_f) feedback are exactly the same. Subsequently, only the active feedback curves are shown in the plot. It is seen
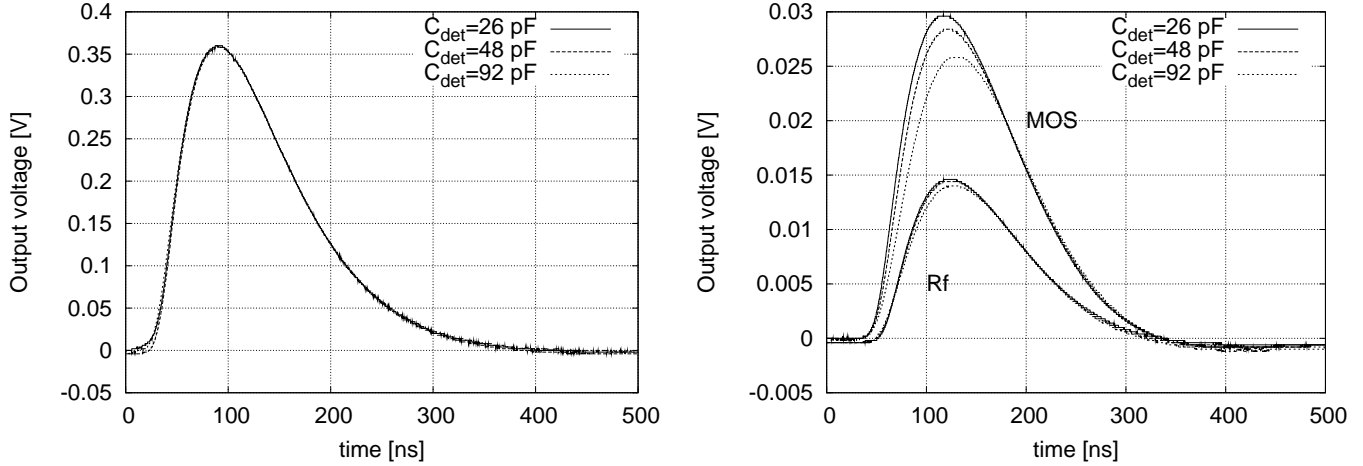
Figure 10: Output pulses for MOS resistor front end channels in physics mode (left) and for MOS and R_f resistor in calibration mode (right), as a function of input capacitance. In calibration mode $Q_\mathrm{in} = 10$ fC, while in physics mode $Q_\mathrm{in} = 3.3$ pC.

that neither the amplitude nor the peaking time ($\sim$70 ns) are sensitive to the value of the input capacitance in this case. In calibration mode the amplitude and the peaking time depend on the input capacitance (C_det). The measurements are in good agreement with Hspice simulations performed for both types of feedback resistors and both gain modes.

The RMS values of the output noise have been measured using a HP3400 true RMS meter. The equivalent noise charge (ENC) as a function of input capacitance is shown in Figure 11. Similar results are obtained for active and passive feedback. Results obtained in the physics (low gain) and calibration (high gain) modes are shown in the same plot. Since the HP3400 has a bandwidth of up to 10 MHz, the values measured may be asured values are generally in agreement with simulations. In particular, in calibration mode the signal to noise ratio of 10 is maintained for input capacitances up to nearly 100 pF. Additional noise measurements have been performed for a few points by measuring the output noise spectra using a HP4195A spectrum analyzer, then integrating numerically to get the RMS noise values. The results of such measurements are shown in Figure 11. They agree within their uncertainties with the HP3400 RMS measurements.

In order to test the effectiveness of the PZC circuit the front end response has been measured as a function of the rate of input pulses. To avoid input charges of both polarities when using a square–wave test signal, the staircase test waveforms are synthesized using the Tektronix AWG2021 waveform generator. It was found that the change in amplitude reaches 2% for input rates of about 3 MHz and is almost insensitive to input capacitance.
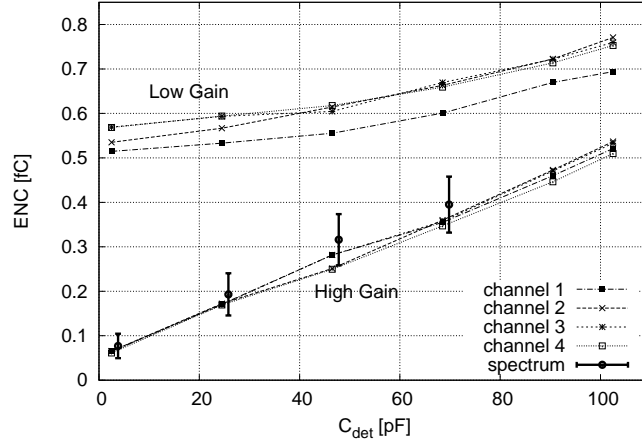
10

Figure 11: Noise ENC measurements obtained with a true RMS meter for the front end with passive feedback.

ADC design Pipeline ADC architecture was chosen for LumiCal data conversion, assuring a good compromise between speed, area, and power consumption. A 1.5-bit per stage architecture was chosen because of its simplicity and immunity to offsets in the comparator and amplifier circuits [13]. Each 1.5-bit stage consist of two comparators, two pairs of capacitors C_s and C_f, an operational transconductance amplifier, several switches and a small digital logic circuit. To improve the ADC immunity to digital crosstalk and other disturbances, a fully differential architecture is used.

Two iterations of design and prototyping of the pipeline ADC have been completed. In the first prototype only the functional ADC unit (i.e. the eight 1.5-bit stages) was implemented. For the second prototype all nine pipeline stages and the input S/H stage were designed. And the digital correction logic was added as well. Additionally, the second prototype included a few slightly different ADC versions. ADCs with and without S/H stage were implemented, as well as ADCs with continues and switched capacitance common mode feedback. Measurement results of the first prototype could be found in [13] while the preliminary results for the second prototype are discussed below.

Preliminary Measurements of the second ADC prototype A photograph of the ASIC containing six slightly different channels is shown in Figure 12. It was first checked that the ADC was fully functional. The Integral Nonlinearity (INL) and the Differential Nonlinearity (DNL) results are shown in Figure 13. The maximum integral nonlinearity is significantly below ±1 LSB while the maximum differential nonlinearity is less then ±0.5 LSB. It may be concluded that both, the INL and the DNL fulfill their respective performance requirements.

An example spectrum for a dynamic circuit performance measurement performed with 40 kHz full-scale (0 dB) pure sinusoidal input signal and sampled at 30 MHz is shown in Figure 14.
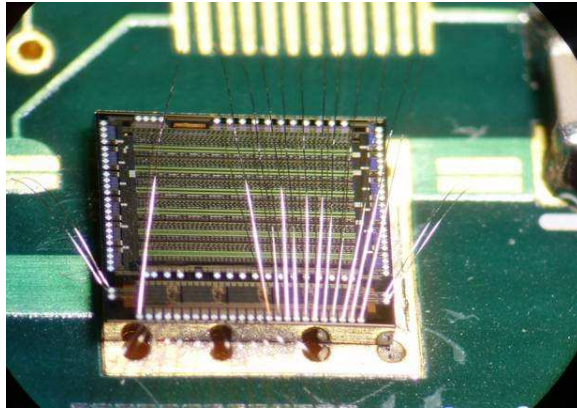
11

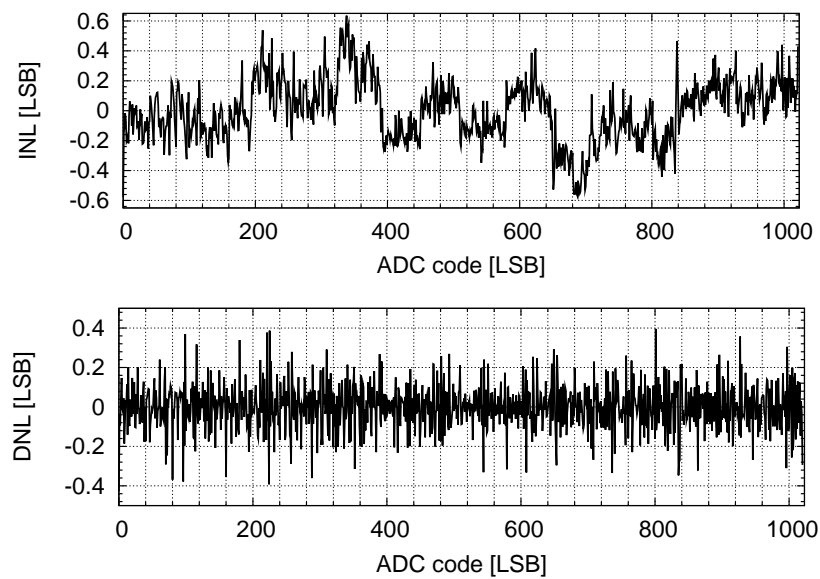Figure 12: Photograph of the glued and bonded ADC prototype.

Figure 13: Static measurements of INL and DNL errors.

It is seen that the harmonic components are small and do not affect the resolution significantly. The signal to noise (SNHR) measured as a function of sampling frequency is shown in Figure 15. An SNHR of about 58 dB is obtained in the frequency range up to almost 25 Mhz. Additional measurements are currently in progress.
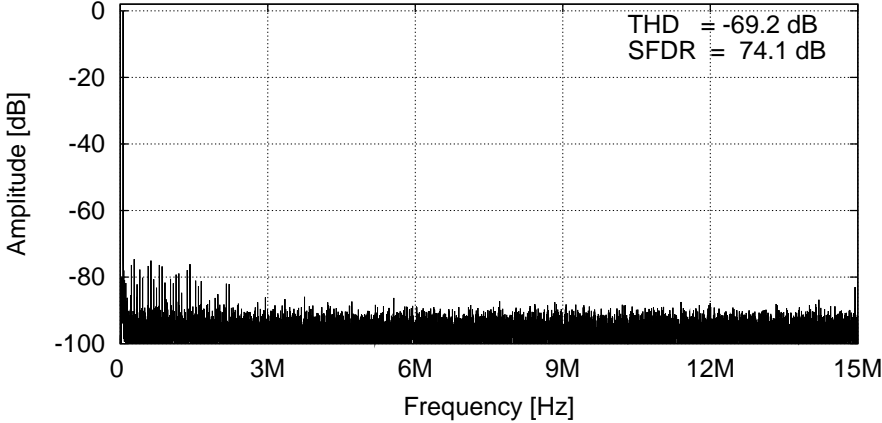
Harmonics   = 10

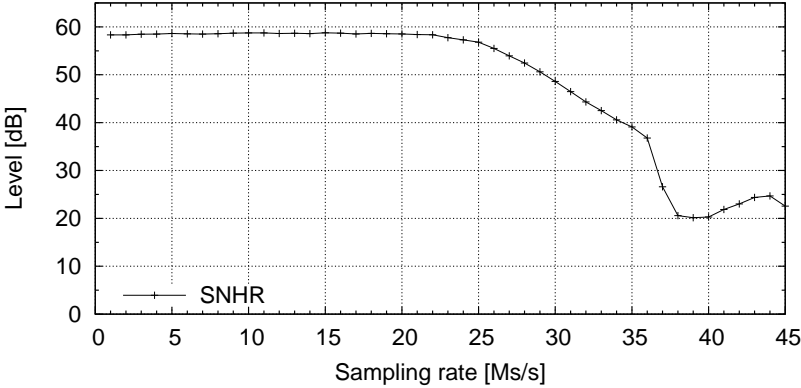Figure 14: Example of FFT measurement with f_{in}=40 kHz and f_{clk}=30 MHz.

Figure 15: ADC performance as a function of sampling rate.

4.1 Full detector chain test preparation

A dedicated printed circuit board (PCB) was produced in order to study the performance of a full read out chain, consisting of silicon sensors, kapton fan-out, and front end electronics (Figure 16). In particular, the test setup is meant to check the functionality
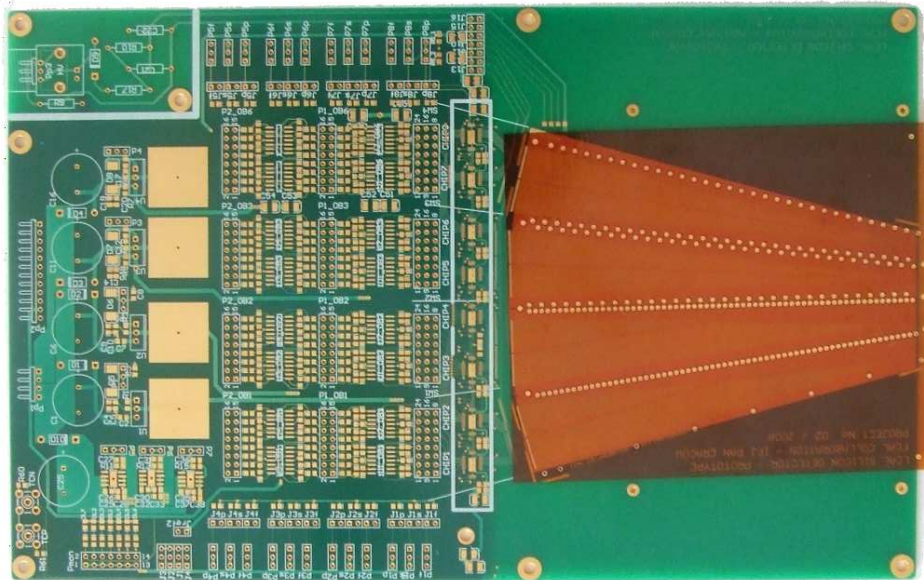

Figure 16: Photo of the PCB and capton foil fan-out.

and quantitative parameters of the front end electronics and to study crosstalk effects due to the sensor and fan-out capacitances. The test setup will contain 4 sectors of silicon sensors (with 64 pads in each sector), kapton foil with fan-out, and up to 16 channels of front end electronics per sector. The number of read out channels is presently limited to eight by the number of channels in the prototype front end ASIC. For this reason, eight ASICs are connected to groups of pads in different regions (and thus with different capacitances) of the sensor.

For a better understanding of crosstalk effects, two types of fan-out were designed and produced. Because the ADC prototypes developed for LumiCal contain only single channels, the conversion in the test setup will be done by external multichannel ADCs. For this reason additional external buffers were added to drive the cables and ADCs inputs. The block diagram of the readout chain is shown in Figure 17 If the test setup confirms good performance of the readout chain, it will be used again in the test beam in the second phase.
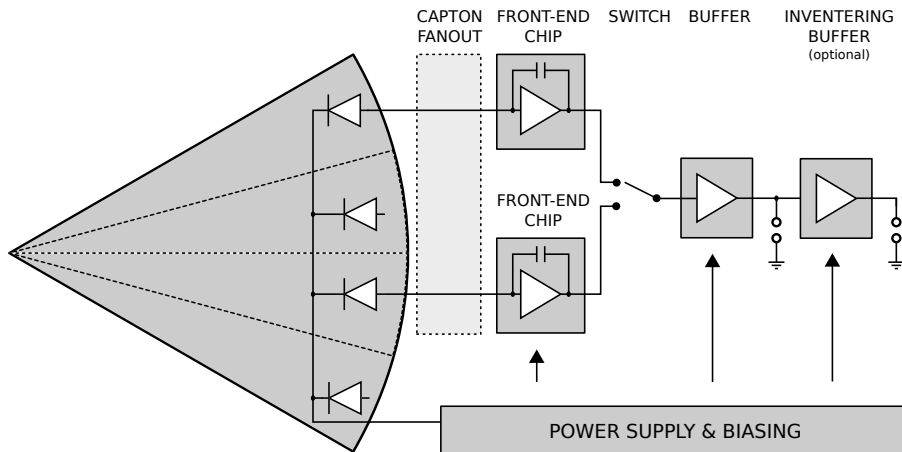
CAPTON FANOUT   FRONT-END CHIP   SWITCH   BUFFER   INVENTERING BUFFER (optional)

FRONT-END CHIP

POWER SUPPLY & BIASING

Figure 17: Block diagram of readout chain.

5 Studies on Radiation Hard Sensors

One of the fields of high priority for BeamCal is a development of large area radiation hard sensors. In this scope the collaboration continued previous studies of Gallium Arsenide and CVD diamond detectors both in the laboratory and in the high intensity electron beam at the DALINAC accelerator. Radiation hardness of a new possible candidate, sapphire, was also studied at the test beam.

Gallium Arsenide (GaAs) Radiation Hardness Studies   The JINR group from DLNP has extended the scope of VFCAL to GaAs sensors. Together with an institute in Tomsk, large area prototype sensors were designed and the first 10 prototypes were produced. To assemble these sensors a special laboratory clean room was prepared. Measurements of the electrical features of the sensors were done both in JINR and at DESY. The performance as a function of the absorbed dose was investigated in a highly intense electron beam at the DALINAC accelerator in 2007. The results of this investigation have shown that GaAs sensors produced in Tomsk have an advantage as radiation-hard sensors in comparison with "classical" silicon semiconductor sensors.

As a development of this investigation, it was decided to study the dependence of the radiation hardness of GaAs sensors samples on technological procedures and variations of the main GaAs parameters like resistivity (3 different values) and the type of material itself (barrier or semi-insulator types). According to these differences the sensors were subdivided into 4 batches. The sensors from the semi-insulator material, with 3 different values of resistivity and 2 types of donor impurity, formed 3 different batches of the sensors, while the sensors with barrier material made up the $4^{t}h$ batch.

Following this request, 64 samples of PAD geometry sensors with different material parameters were designed and produced by the Tomsk institute. The measurements have been done at DALINAC accelerator beam in December 2008. Six sensors from the first 3 batches were exposed with a dose rate in the range from 20 to 400 kGy

per hour in periods of 0.5 to 1 hour. The main detector characteristic - the charge collection efficiency (CCE) - was measured in between. A clear dependence of the radiation hardness on the concentration of the donor was observed. The dependence of the charge collection efficiency on the absorbed dose for the sensors with different donor concentrations is shown in Figure 18.
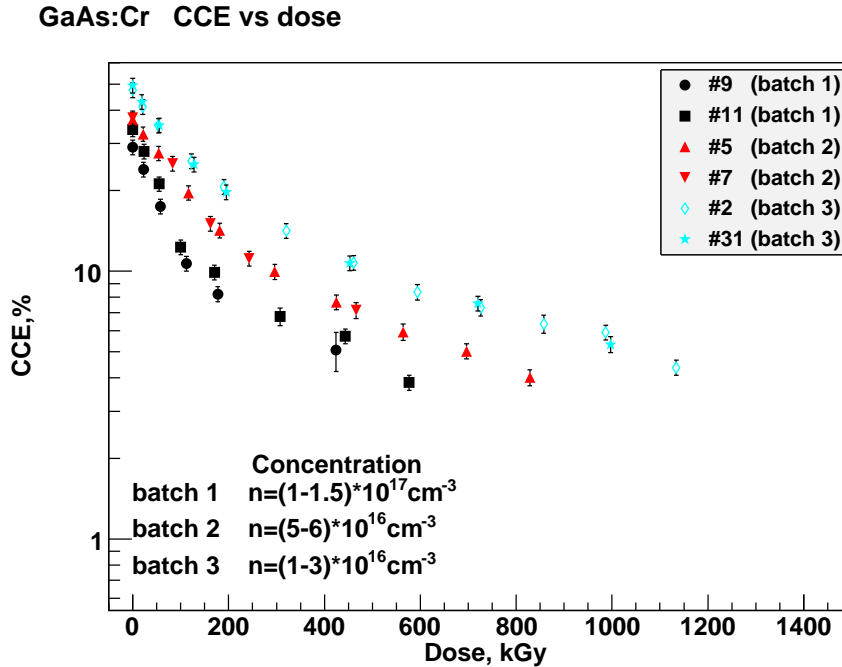
GaAs:Cr CCE vs dose

Figure 18: The CCE as a function of the absorbed dose for the GaAs sensors with different donor concentrations. The donor impurity is Te for the batches 1 and 2 and Sn for batch 3.

For a more detailed study of sensor radiation hardness on donor concentration 28 new samples of GaAs sensors with a different donor concentration were ordered and produced in Tomsk in 2009. These samples will be irradiated by different sources (DALINAC, synchrotron radiation source, etc.) in 2010.

Radiation hardness of scCVD Diamond   In December 2008 we had continued irradiation of the single crystal CVD diamond detector, which was first done in June 2007, up to the dose of 10 MGy. Dependence of CCD on the absorbed dose, measured during beam interruptions using ^{90}Sr source setup, is shown in the Figure 19. Blue dots correspond to irradiation in 2007, and red dots to 2008 testbeam irradiation. It is clearly seen that no annealing of the damaged crystal during almost 1.5 years is observed. It should be noted that during this time the detector was intensively tested in the laboratory, including several TSC tests at high temperatures.
We have studied the mechanism of charge collection in the radiation damaged diamond sensor. It was found that in the damaged detector, operating under a bias voltage, strong

polarization develops in the bulk of the sensor material. This polarization, together with trapping of the charge carriers, is responsible for the drop of charge collection efficiency. Regular change of the bias voltage polarity eliminates the polarization and speeds up the filling of long-living traps (*pumping* or *priming* effect). This way a significant part of efficiency can be recovered. It can be seen for example in the Figure 21, where time evolution of the signal from the 10 MGy damaged detector is presented for different operating conditions. Before each measurement the sensor was irradiated by UV light to free the traps and ensure the same starting conditions. Red dots represent slow development of polarization when at steady state efficiency drops to about 30 μm, which corresponds to the last point in Figure 19. Other dependencies shown in Figure 21 illustrate efficiency recovery at different operating conditions.

We also tested the assumption that the part of detector efficiency which couldn't be recovered by above methods is caused by the presence of short-lived traps. For that purpose we built a new testbeam setup that allowed remotely-controlled fast movement of the detector from the beamline to the position inside the ^{90}Sr setup. We have observed the tail of rapid variation of the signal size correspondent to the sharp change of irradiation intensity. This study needs to be continued with improved setup time resolution.
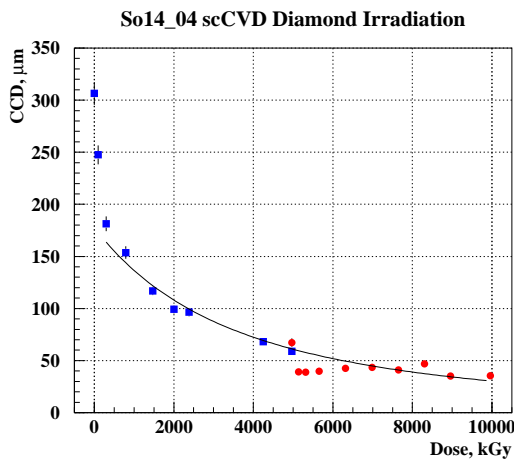

Figure 19: CCD of diamond sensor vs absorbed dose. Blue points - irradiation-2007, red points - additional irradiation in Dec 2009.
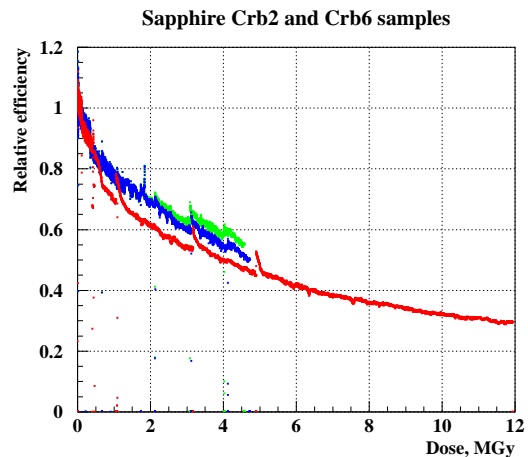
Figure 20: Relative Charge Collection Efficiency of Sapphire sensors as a function of the absorbed dose.

Study of Sapphire Radiation Hardness During December 2008 testbeam campaign we had studied the radiation hardness of another large band-gap material, sapphire. Several monocrystalline sapphire plates of $10 \times 10 \times 0.5$ mm^3 size were covered with Al-Ti-Au and pure Al metallization from both sides and irradiated at the DALINAC test beam up to 12 MGy of the absorbed dose. Relative charge collection efficiency, as

estimated from the detector current measurements, is shown in Figure 20 as a function of the absorbed dose. It is seen that the sensors kept about 30% of their initial efficiency after a dose of 12 MGy. This makes them one of the most radiation hard materials known so far.

Unfortunately, a low initial charge collection efficiency (most probably due to insufficient purity of the feed) didn't allow us to measure signal parameters directly. Nevertheless obvious advantages like extremely small leakage current (a few pA before and after irradiation), low cost and availability at large wafer sizes make further studies of sapphire worthwhile.
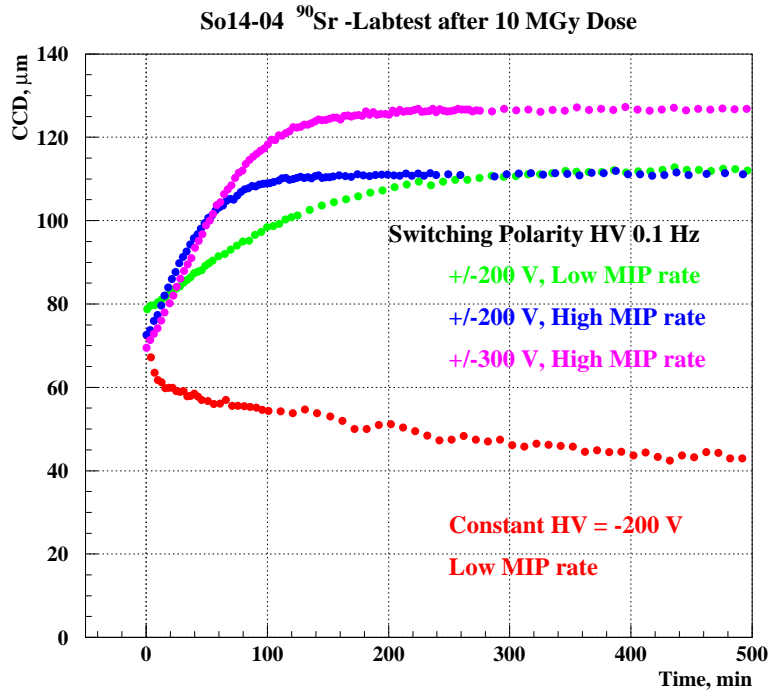

Figure 21: Time evolution of damaged diamond sensor CCD under ^{90}Sr-source irradiation. See text for details.

Future Plans In the future the main goal will be the system test of all components developed by collaboration at the realistic test beam conditions. For that purpose we are planning to build a flexible test structure (see Figure 22) which includes tungsten plates and sensor planes. Both LumiCal and BeamCal sensors (or their combinations) are going to be tested together with multichannel readout electronics. Already available GaAs-based BeamCal sensor plane prototype is shown in Figure 23. It has still to be equipped with the fanout structure connecting individual pads with readout electronics. Radiation hardness studies of BeamCal components will be continued. For example, in the beginning of 2010 we are planning to irradiate thin CVD diamond films (about

100 μm thickness) to study the dependence of residual charge collection efficiency on the thickness of the detector. Another promising candidate, sapphire, will be further studied, provided that cleaner sapphire substrates will be found.
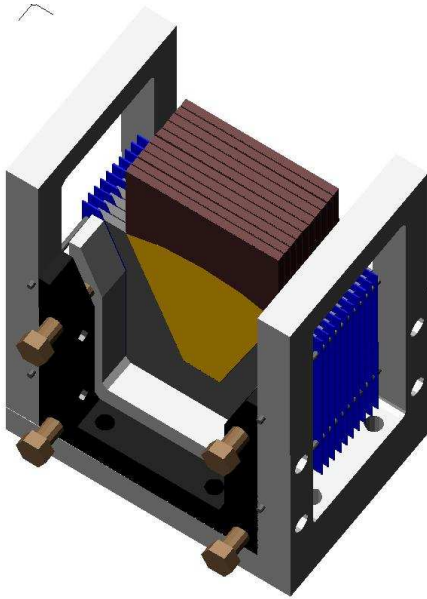

Figure 22: Design of the Test Structure for the future system tests of the BeamCal and LumiCal sensors.
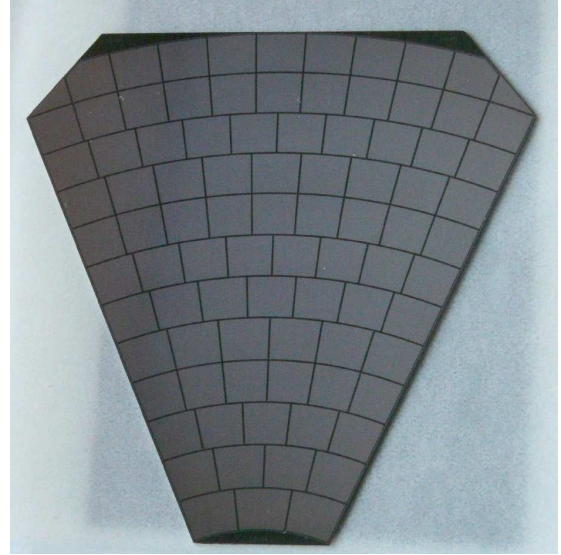

Figure 23: Prototype of GaAs multipad sensor for BeamCal.

5.1 Sensor application at FLASH

Eight sensors designed for long-term investigation under real accelerator conditions are used in the Beam Halo Monitor (BHM) system near the beam dump at the Free-Electron Laser Hamburg (FLASH) (Figure 24) [14] - the prototype for an X-ray free-electron laser (XFEL). After the upgrade in 2009 the maximal electron beam energy will be 1.2 GeV, the beam will be grouped into bunches of up to 3 nC with a repetition rate of up to 3 MHz, and the total number of bunches per train will be 800. The bunch train repetition rate will be up to 10 Hz. Laser pulses in the picoseconds region with wavelengths of down to 6.5 nm will be produced. The BHM system will be part of the beam dump diagnostics, which serves for the adjustment of beam parameters and alarm signals generation.

Four polycrystalline CVD diamonds, of dimensions $12 \times 12 \times 0.3$ mm^3, and four artificial monocrystalline sapphires with dimensions $10 \times 10 \times 0.5$ mm^3, covered with Ti-Pt-Au metallization from both sides, have been installed inside the last section of the electron beam pipe within the hollow cylinders as shown in Figure 25. The diamond and sapphire sensors alternate and are uniformly distributed in the tangential direction. The sensors are operated like solid state ionization chambers. A bias voltage of up to a few hundred volts is applied. The bias voltage supply is located $\sim$ 50 meters away from the sensors.
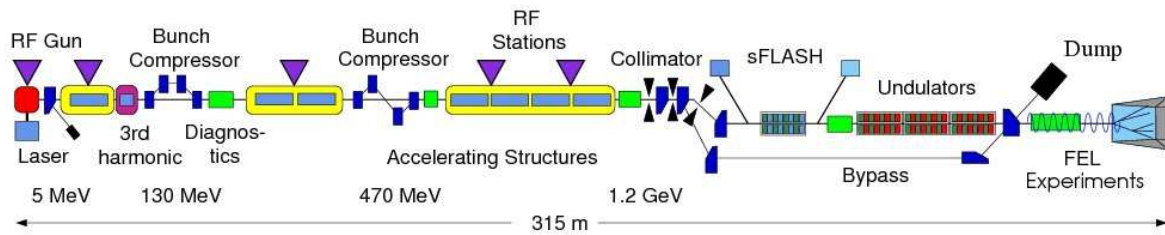
19

Figure 24: Schematic view of the FLASH.

Four meters away from the sensors a bias voltage filter with charge storage capacitors is installed. The length of the signal line is about 50 meters. The signals are digitized with a sampling ADC. The first signals from the BHM sensors were observed during the test run in September this year. All the sensors were operational and have shown a clear response to the beam.
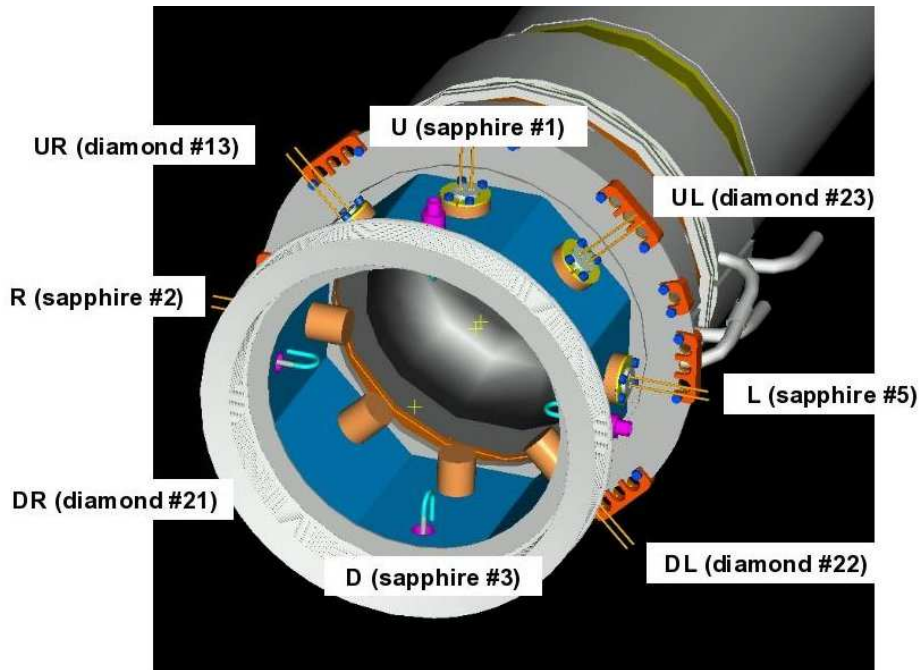

Figure 25: The position of BHM sensors at the end of the beampipe.

FLASH will continue operation in spring 2010. The performance of diamond and sapphire sensors in the environment of an electron beam with short intense pulses will be investigated, and long-term stability under such conditions will be checked.

6 Conclusion

This paper summarizes the VFCAL EUDET project and discusses the progress achieved. All milestones have been already accomplished, relevant EUDET reports and memos are written. Recent examples of achievements are the prototyping of the laser alignment system, manufacturing and performance tests of multichannel silicon sensor prototypes for LumiCal, performance measurements of the front end electronics and 10-bit ADC converter ASICs and studies on the radiation hardness of BeamCal sensors candidates. Infrastructure created within EUDET activity has been an essential tool to make all these achievements possible.

In the future the main goal will be the system test of all components developed by collaboration at the realistic test beam conditions.

Acknowledgement

References

[1] H. Abramowitcz et al., "Instrumentation of the Very Forward Region of a Linear Collider Detector", IEEE Transactions ofNuclear Science, 51, 2004.

[2] ILC Global Design Effort and World Wide Study. "International Collider Reference Design Report", 2007, http://linearcollidder.org

[3] ILD Concept Group, "Letter of Intent for the International Large Detector", 2009, http://ildilc.org

[4] J. Mnich, "Detectors for a Linear Collider", EUDET-Report-2007-02, 2007.

[5] W. Daniluk et al., "Laser Alignment System for LumiCal", EUDET-Report-2008-05, 2008.

[6] L. Zawiejski et al., "Laser Alignment System For Luminosity Detector LumiCal", in *Proceedings of the Workshop of the Collaboration on Forward Calorimetry at ILC*, Vinca Institute of Nuclear Sciences, September 2008.

[7] A.F. Fox-Murphy et al., Nuclear Instruments and Methods in Physics Research A 383 (1996) p.229.

[8] J.R. Green, "Development of a Prototype Frequency Scanning Intererometric Absolute Distance Measurement System for the Survey&Alignment of the International Linear Collider". PhD thesis, University of Oxford, 2007.

[9] Hai-Jun Yang et al., Nuclear instruments and Methods in Physics Research A 575 (2007) p.395

[10] M. Warden et al., "MONALISA: A precise system for accelerator component position monitoring", EUROTEV-Report-2008-08.

[11] J. Blocki et al., "Silicon Sensors Prototype for LumiCal Calorimeter", EUDET-Memo-2009-07, 2008.

[12] S. Schuwalow, "Forward Calorimetry sensor test facilities", EUDET-Memo-2008-32, 2008.

[13] M. Idzik et al., "Status of LumiCal readout electronics", EUDET-Report-2008-08, 2008.

[14] FLASH web page, http://flash.desy.de/